Anti-Islanding Detector based on a Robust PLL

Stefano Bifaretti
Department of Industrial Engineering
University of Rome Tor Vergata
Rome, Italy
bifaretti@ing.uniroma2.it

Alessandro Lidozzi, Luca Solero, Fabio Crescimbini
Department of Engineering
University RomaTre
Rome, Italy
lidozzi@uniroma3.it

Abstract- **International Standards impose to Distributed Energy Resources, connected to the grid by an inverter, to detect an islanding condition within a suitable time interval. In this paper a Phase Locked Loop (PLL), based on a third-order prediction-correction filter, is proposed to implement an islanding detector with reduced detection time. Such a feature is obtained using the estimation of the grid angular frequency and acceleration provided by the PLL with a negligible time delay. The proposed approach is implemented on an industrial grade DSP and validated through the experimental comparison among different detection methods, such as Rate of Change of Frequency (ROCOF) and Slip Mode frequency Shift (SMS). The combined use of ROCOF and SMS is also illustrated and discussed.**

I. INTRODUCTION

Islanding is defined as the condition in which a Distributed Energy Resource (DER) continues to supply power to local loads even if the grid is disconnected. According to IEEE 929-2000, IEEE 1547.1, VDE 0126.1.1 and IEC 62116 Standards, for safety reasons, grid-connected DER systems have to identify a situation of grid fault and disconnect from the grid within a fixed time interval, in range 0.1s to 2s depending on the applicable standard and on the type of fault [1]-[5]. Recent Italian standard CEI-021 requires a lower detection interval, equal to 0.05s, for over/under frequency protection [6]. The typical block diagram of the DER based on a single-phase grid-connected converter, incorporating the anti-islanding detection, is shown in Figure 1.

Several islanding detection methods, which can be classified in passive [7], active [8] or hybrid [9], have been proposed in literature. The first ones are based on the detection of an abnormal operating condition of at least one of the electrical parameters of the grid (voltage, frequency, phase) without injecting any perturbation into the grid so that the power quality is not affected. On the contrary, active methods detect the response of the grid after the injection of an opportune disturbance. Hybrid methods use the combination of an active and a passive detection method by injecting a perturbation into the grid only when the passive detector suspects the islanding condition.

The most important parameter for evaluating an islanding detection method is the extension of the Non-Detection Zone (NDZ) [10]-[12]. Based on such criterion, active methods present a smaller NDZ than passive ones, as they are able to detect islanding conditions even in case of exact power balance between supply and load; however, they can negatively affect the power quality.

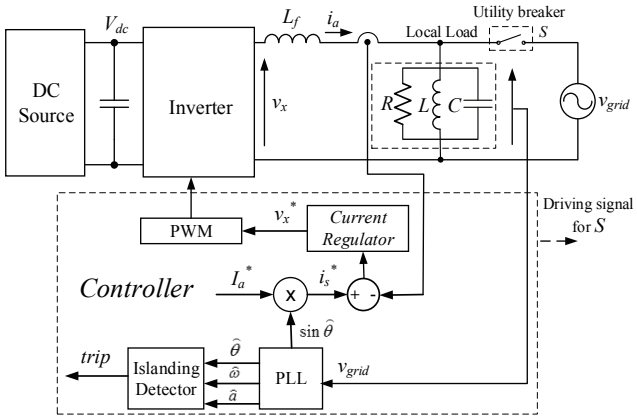

Figure 1. Block diagram of the grid-connected converter.

The hybrid methods aim to reduce the disadvantages of both passive and active methods: in particular, they mitigate the negative effects on the grid introduced by active ones while maintaining a NDZ smaller than passive; however, the islanding detection time becomes longer than other techniques.

The main passive detection methods employed in grid-connected converters are:

- Over/Under Voltage (OUV)
- Over/Under Frequency (OUF)
- Voltage Harmonics
- Phase Jump

OUV and OUF are rarely employed as anti-islanding detection methods due to their large NDZ, which strongly depends on load conditions [7], [10]. However, commercial grid-connected converters and utility interface devices always incorporates OUV and OUF for monitoring purposes. The Voltage Harmonics method [13] is based on the observation that when the grid becomes disconnected, the current harmonics produced by the converters will flow on

the local load whose impedance is much larger than the grid impedance, so producing larger voltage harmonics. In this method is quite difficult to choose a trip threshold that guarantees a fast and reliable detection time as the harmonic distortion strongly depends on local loads. The Phase Jump detection method is based on monitoring the phase difference between current and voltage, which is near to zero when the utility voltage is connected while it could present a significant variation during a disconnection [10]. However, if a fast Phase Locked Loop (PLL) is used, such variation is negligible making this detection method ineffective [7].

Another interesting passive method, denoted as Rate Of Change Of Frequency (ROCOF), is based on the measure of the derivative of the angular frequency. Such a technique is widely used, in particular for large power DER using synchronous generators [14], due to the shorter detection times and reduced NDZ than other passive methods [14]-[15]. However, the use of ROCOF as a resident islanding detection method for small power DER, such as Photovoltaic generators, has been not widely investigated in literature as the other passive methods.

Amongst resident active methods, the most popular are:

- Impedance estimation
- Slip Mode frequency Shift (SMS)
- Active Frequency Drift (AFD)
- Sandia Frequency Shift (SFS)

The Impedance estimation method [16] is based on the injection of a current harmonic disturbance at a specific frequency and detecting the resulting voltage harmonic at the same frequency; then the impedance calculation is used to determine the trip. Such a method requires an additional monitoring PLL, tuned on the injected frequency; furthermore, the detection effectiveness strongly depends on the load. A recent paper [17] has proposed a novel solution that almost eliminates the above-mentioned drawbacks of the grid impedance estimation method. The other methods, listed above, use a positive feedback in order to produce instability only in case of a grid disconnection. In particular, SMS introduces a perturbation on the inverter output current phase angle, while AFD and SFS force a change of the frequency. Such feedback-based methods are demonstrated to be very effective and a good compromise between detection time and power quality degradation [18]. However, in order to reduce the islanding detection time and to comply with the new CEI-021 Italian standard, this paper proposes the combined use of specific islanding detection methods and a PLL with a loop filter based on a third-order linear and time-invariant observation model. Despite of the traditional PLL, the proposed system provides also the estimation of angular acceleration, in addition to the estimation of the grid angle and frequency. Moreover, the frequency is estimated with a negligible time delay, so a very rapid detection is obtained. The angular acceleration estimation is used to implement the islanding detector, based on the Rate Of Change Of Frequency of the grid, without performing an explicit derivative of the frequency [19] and, thus, without increase the computational complexity of the controller. The performances and the robustness of the Steady-State Linear Kalman Filter (SSLKF) based PLL have been already proven for standard three-phase grid-connected systems in [20]-[21]. In this paper the estimations provided by SSLKF-PLL are used to evaluate the performance of different islanding detection methods, such as ROCOF, SMS and the combination of both (SMS+ROCOF). The comparison has been performed, at first, by Matlab/Simulink simulations accounting, as required by the most important international Standard, a RLC load for different Q values. The proposed method has been implemented on a Texas Instruments TMS320F28335 based board employed to control the grid-connected inverter laboratory prototype. Some major experimental results and a comparison versus two popular islanding detection methods, have confirmed the validity of the proposed approach.

II. PLL MODEL

Figure 2 shows the block diagram of a single-phase PLL system which uses, as a Phase Detector, the vector product between the grid measured voltage phasor and the one estimated by the PLL. Such a system is derived from a three-phase PLL, by adding an Orthogonal Signal Generator (OSG) that produces two-quadrature signals v_α and v_β. The OSG can be implemented using, for example, a Second-Order Generalized Integrator (SOGI) [22]. The signal error e furnished by the vector product can be approximated by its sine and thus, using a small signal analysis, represents the error between the grid voltage phasor angle θ_{grid} and the estimated angle $\tilde{\theta}_{grid}$:

$$\begin{aligned} e &= \frac{v_\beta \cdot \cos\tilde{\theta}_{grid} - v_\alpha \cdot \sin\tilde{\theta}_{grid}}{V_S} = \\ &= \sin\theta_{grid} \cdot \cos\tilde{\theta}_{grid} - \cos\theta_{grid} \cdot \sin\tilde{\theta}_{grid} = \\ &= \sin(\theta_{grid} - \tilde{\theta}_{grid}) \cong \theta_{grid} - \tilde{\theta}_{grid} \end{aligned} \quad (1)$$

where V_S is the module of the grid voltage phasor, while v_α and v_β are its real and imaginary components, referred to a stationary reference frame $\alpha\beta$. The sine and cosine of the angle $\tilde{\theta}_{grid}$ are calculated by means of a numerical procedure or a look-up table.

The Loop Filter is generally implemented with a Proportional Integral (PI) regulator, providing the estimated value of the angular frequency $\tilde{\omega}_{grid}$, followed by an integrator, which provides the estimated phase $\tilde{\theta}_{grid}$.

In this paper a deterministic prediction-correction filter, derived by the SSLKF, is used as a Loop Filter. The prediction-correction filter has been described in [20]-[21] for three-phase grid-connected applications and its performance on the estimation of the phase and frequency proven even when abnormal operating conditions of the grid occur. In the present contribution, a deterministic filter structure is described directly as the prediction model followed by a correction one, both expressed by their discrete-time form, as the PLL system has to be implemented in a digital device.

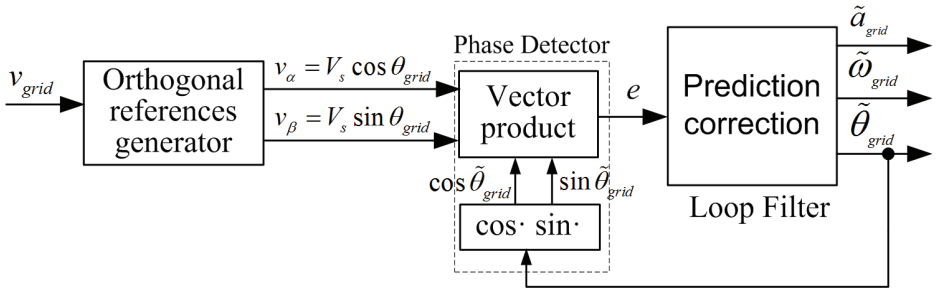

Figure 2. Block diagram of a single-phase PLL based on the vector product.

The third-order physical prediction model, based on the electrical grid equations, can be written as follows:

$$\begin{aligned} \boldsymbol{x}_n &= \boldsymbol{A}\boldsymbol{x}_{n-1} \\ y_n &= \boldsymbol{c}^T \boldsymbol{x}_n \end{aligned} \tag{2}$$

where:

$$\boldsymbol{x} = \begin{bmatrix} \theta_{grid} \\ \omega_{grid} \\ a_{grid} \end{bmatrix} \qquad \boldsymbol{A} = \begin{bmatrix} 1 & T & T^2/2 \\ 0 & 1 & T \\ 0 & 0 & 1 \end{bmatrix} \qquad \boldsymbol{c}^T = [1 \quad 0 \quad 0],$$

being n the sampling instant, T the sampling interval, θ_{grid} the grid voltage angle, ω_{grid} the grid angular frequency, a_{grid} the grid angular acceleration.

On the basis of dynamic model (2), prediction-correction filter performs the following two steps:

1) state prediction at the subsequent sampling instant

$$\tilde{\boldsymbol{x}}_n = \boldsymbol{A}\hat{\boldsymbol{x}}_{n-1}$$

2) correction of predicted state on the basis of the prediction phase error $e_n = \theta_n - \boldsymbol{c}^T \tilde{\boldsymbol{x}}_n$

$$\hat{\boldsymbol{x}}_n = \tilde{\boldsymbol{x}}_n + \boldsymbol{g}e_n.$$

Coefficients g_1, g_2 and g_3 of correction vector

$$\boldsymbol{g}^{\mathrm{T}} = [g_1 \; g_2 \; g_3]$$

can be selected by imposing the poles of the transfer function. Combining the prediction equation at sampling instant n with the correction equation, at the sampling instant $(n-1)$, the following dynamic equation of the prediction-correction filter is obtained:

$$\tilde{\boldsymbol{x}}_n = \hat{\boldsymbol{A}}\tilde{\boldsymbol{x}}_{n-1} + \boldsymbol{A}\boldsymbol{g}\theta_{n-1} \tag{3}$$

being

$$\hat{\boldsymbol{A}} = \boldsymbol{A}\left(\mathbf{I} - \boldsymbol{g}\boldsymbol{c}^{\mathrm{T}}\right).$$

The prediction-correction filter poles can be imposed, on the base of the desired bandwidth, by equating the eigenvalues of the characteristic equation associated to dynamic matrix $\hat{\boldsymbol{A}}$ to those of a third-order discrete filter.

Transforming in z-domain the discrete-time eq. (3) and choosing, as input, the measured grid angle θ, the following transfer functions $G_\omega(z)$ and $G_a(z)$ are obtained:

$$\frac{\tilde{\omega}}{\theta_{grid}} = G_\omega(z) = \frac{(g_2 + Tg_3)z^2 - 2(g_2 + Tg_3)z + g_2}{z^3 + c_2 z^2 + c_1 z + c_0} \tag{4}$$

$$\frac{\tilde{a}}{\theta_{grid}} = G_a(z) = \frac{g_3(z-1)^2}{z^3 + c_2 z^2 + c_1 z + c_0} \tag{5}$$

being c_0, c_1 and c_2 defined as in (6).

$$\begin{aligned} c_2 &= g_1 + g_2 T + g_3 T^2/2 - 3, \\ c_1 &= -2g_1 - g_2 T + g_3 T^2/2 + 3, \\ c_0 &= g_1 - 1. \end{aligned} \tag{6}$$

A third-order discrete filter, with a sampling period T, can be characterized by a negative real pole of module $\rho_0 = \mathrm{Exp}(-\omega_n RT)$ and a pair of complex poles of module $\rho_1 = \mathrm{Exp}(-\omega_n T\cos\phi)$ and phase $\varphi = \omega_n T \sin\phi$.

Parameters ω_n, R and ϕ are used to set the desired bandwidth, transient and steady-state response. The proposed filter can be designed, in the same way, imposing the eigenvalues of the characteristic equation equal to those of the discrete filter ($\lambda_1 = \rho_0$, $\lambda_{2,3} = \rho_1 \mathrm{Exp}(\pm j\varphi)$) so the coefficients of the characteristic equation become:

$$\begin{aligned} c_2 &= -2\rho_1 \cos(\varphi) - \rho_0, \\ c_1 &= \rho_1\left[2\rho_0 \cos(\varphi) + \rho_1\right], \\ c_0 &= -\rho_0 \rho_1^2. \end{aligned} \tag{7}$$

Finally, from (6) and (7), the elements of the vector $\boldsymbol{g}$ can be calculated as:

$$\begin{aligned} g_3 &= \frac{c_1 + c_0 + c_2 + 1}{T^2}, \\ g_2 &= \frac{c_1 - c_0 + 3c_2 + 5}{2T} - Tg_3, \\ g_1 &= c_2 + 3 - Tg_2 - g_3 T^2/2. \end{aligned}$$

III. ANTI-ISLANDING APPROACH

The block diagram representing the discrete-time implementation of the ROCOF anti-islanding method is illustrated in Figure 3.

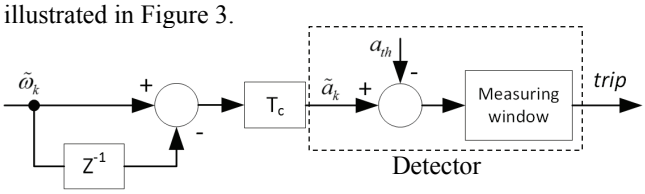

Figure 3. Block diagram of ROCOF method.

The estimated angular acceleration is achieved by the derivative of the estimated angular frequency, provided by the PLL, as follows:

$$\tilde{a}_k = \frac{\tilde{\omega}_k - \tilde{\omega}_{k-1}}{T_c}$$

The trip signal is then generated when the angular acceleration becomes larger than a fixed trip threshold a_{th} for a suitable time interval defined in the measuring window.

As the PLL, described in section II, provides also the estimation of the angular acceleration, without performing any explicit derivative of the grid frequency that normally produces a very noisy output signal, this paper proposes the usage of $\tilde{a}_{grid}$ to perform the ROCOF algorithm.

Using (1), the linearized PLL model, shown in Figure 4, is obtained.

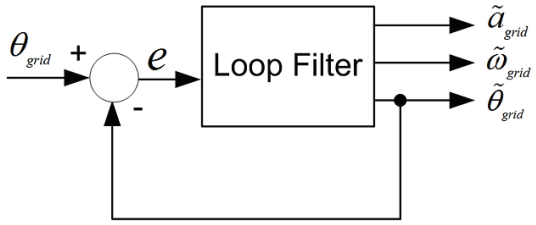

Figure 4. PLL linearized model.

The equivalent electrical model, accounting only the fundamental harmonic, of the inverter connected to a local load Z_L and to the grid is depicted in Figure 5, where the converter and the grid are modeled, respectively, as a current-controlled current source and a voltage source, whilst Z_g represents the grid impedance.

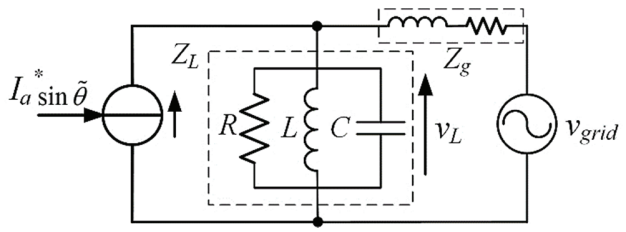

Figure 5. Equivalent electrical model.

Using the approach shown in [23], the linearized PLL model, including the grid interaction, is composed, in grid-connected mode, of one negative feedback loop, due to the contribution of the grid voltage, and one positive feedback loop determined by the inverter current controller, which acts as a disturbance and tends to drive the PLL away from its equilibrium point. In islanding condition, Z_g becomes infinite so, as illustrated in Figure 6, only the positive feedback loop remains active. Considering a RLC parallel load, the feedback transfer function H can be expressed as follows [24]:

$$H = \frac{-2Q}{\omega_r} I_a^* R_L$$

being Q the load quality factor and ω_r the resonant frequency.

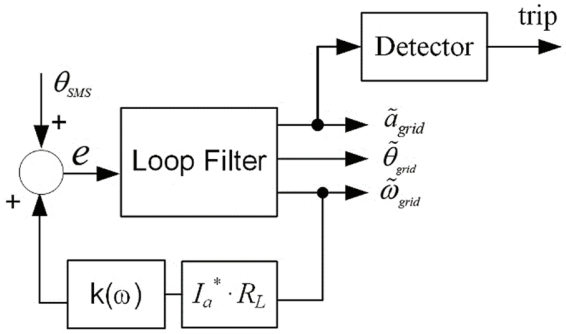

Figure 6. PLL model in islanding mode.

The closed-loop transfer function of the PLL model in islanding mode is calculated using (4) as follows:

$$W(z) = \frac{G_\omega(z)}{1 - G_\omega(z)H} = \frac{(g_2 + Tg_3)z^2 - 2(g_2 + Tg_3)z + g_2}{z^3 + c_{2w}z^2 + c_{1w}z + c_{0w}} \quad (8)$$

being

$$c_{2w} = c_2 - H(g_2 + Tg_3)$$
$$c_{1w} = c_1 + H(2g_2 + Tg_3)$$
$$c_{0w} = c_0 - Hg_2$$

As it can be observed from (8), when the islanding occurs, the poles of $W(z)$ moves from the positions defined in (6) making the system stability depending on the load conditions and on the current reference. Since it cannot be assured that the system results unstable, thus permitting a fast islanding detection, for any parameters values, the phase of the injected current is intentionally shifted by a small angle θ_{SMS} to drift the PLL from a possible equilibrium point.

This latter permit to evaluate the islanding method based on the combination of ROCOF with an intentional phase shift (SMS+ROCOF) which has not previously investigated in literature.

IV. SIMULATION RESULTS

The behavior of the proposed method has been evaluated, at first, through Matlab/Simulink/SimPowerSystem tool using the electrical model shown in Figure 1. The model is composed of an H-Bridge inverter, powered by a 400V DC source, connected to a local *RLC* load and to a 50 Hz 230V AC grid through a filter inductance L_f. A controlled switch *S* has been used in order to emulate the islanding condition at a

desired time instant. The inverter controller includes the PLL algorithm, illustrated in section II, which furnishes a sinusoidal reference signal for the current regulator and the grid state variables estimation $\hat{\boldsymbol{x}}_n$, employed by the islanding detector procedure.

TABLE I. ELECTRICAL AND CONTROL PARAMETERS

Name	Description	Value	Unit
V_{DC}	DC Voltage	400	[V]
L_f	Filter inductance	1.4	[mH]
ω_h	Filter resonant frequency	2π*10	[rad/s]
R	Filter real pole position tuning	1	-
ϕ	Filter imaginary pole position tuning	45	[°]
BW	Approx. PLL Bandwidth	17	[Hz]
f_s	Sampling Frequency	12.8	[kHz]

Such a detector produces a suitable high-level logic signal, denoted as *trip*, when the islanding condition occurs. The dead-beat current control system, described in [25], is employed as a grid current regulator.

The parameters used in the simulation model are summarized in Table I. To evaluate the performance of the proposed method, a comparison among Over/Under (O/U) frequency, ROCOF, SMS and the combination of both (SMS+ROCOF) Islanding Detection methods are considered. The comparison has been performed accounting either a pure resistive load or a RLC load, with different Q values, in order to comply with the different international Standards. The trip thresholds imposed for O/U frequency and for SMS are set to (50±0.3) Hz, as required by CEI 0-21 Standard, while the trip thresholds for ROCOF are imposed to ±1.7 Hz/s.

Table II shows the results of the detection times obtained by the different methods at the specified load condition. As it can be noticed, ROCOF and SMS+ROCOF present very low detection time intervals; however, the combined SMS+ROCOF technique is not affected by NDZ for any of the considered load conditions.

TABLE II. COMPARISON OF DETECTION TIMES

Load Condition		Detection Times [ms]			
Q	I_a^* [A]	O/U Frequency	SMS	ROCOF	SMS + ROCOF
0.25	1	4.3	4.1	2.6	2.5
0.55	1	5.1	4.9	3.1	2.9
1.4	1	13.6	13.3	3.8	3.7
2.5	1	15.2	14.9	4.6	4.3
2.5	22.5	NDZ	NDZ	14.6	15.1
R 300 Ω	1.1	NDZ	NDZ	NDZ	15.9

V. EXPERIMENTAL RESULTS

The behavior of the proposed method has been experimentally demonstrated using the experimental setup illustrated in Figure 7. The hardware prototype is composed of an H-Bridge inverter, built with IRFP264 MOSFETs, a filter inductance L_f, a local *RLC* load and a 400V DC source. A Texas Instruments TMS320F28335 Digital Signal Controller (DSC) has been employed to implement the inverter controller, including the PLL algorithm and the islanding detectors. A single-pole relay *S*, driven by the DSC, has been used to emulate the islanding condition at a desired time instant. The same parameters adopted in the simulation model and listed in Table I have been employed also in the experimental setup, except for the PLL bandwidth that has been imposed to 10Hz in order to obtain a strongest filtering action.

Different experimental tests have been performed accounting a pure resistive load or a resonant load with Q=1.4; in particular, the test procedures have been performed setting an opportune current reference I_a^* which is able to replicate, for each of the considered loads, the same grid voltage as before the grid disconnection. A first test has been performed accounting a 30Ω pure resistive load with a current reference I_a^* =10.5A in order to produce the same voltage at PCC after grid disconnection. Figure 8a, 8b and 8c show the achieved experimental results, respectively, for SMS, ROCOF and SMS+ROCOF, having imposed the frequency trip thresholds equal to (50±0.3) Hz for SMS and equal to ±1.7 Hz/s for ROCOF and SMS+ROCOF methods. For SMS and SMS+ROCOF methods, an intentional phase shift, equal to 6°, has been introduced. In Figure 8 are shown the logic signals *Grid disconnected* and *Trip*, both generated by a Digital-to-Analog Converter, and respectively representing the status of relay *S,* used to emulate the islanding condition, and the islanding detector trip. The time interval elapsed between the falling edge of *Grid disconnected* and the rising edge of *Trip* represents the measurement of the detection time interval. In both Figure 8 and Figure 9, the depicted grid voltage is acquired on the grid side of the controlled islanding contactor *S*. A subsequent experiment has been performed considering a RLC load with Q=1.47 (R=30 Ω, L=65mH, C=156μF), the same detector thresholds and current reference used in the previous test. Experimental results are illustrated in Figure 9a, 9b and 9c respectively for SMS, ROCOF and SMS+ROCOF methods. As it can be noticed from Figure 9c, even supplying the resonant load, the detection time is particularly fast.

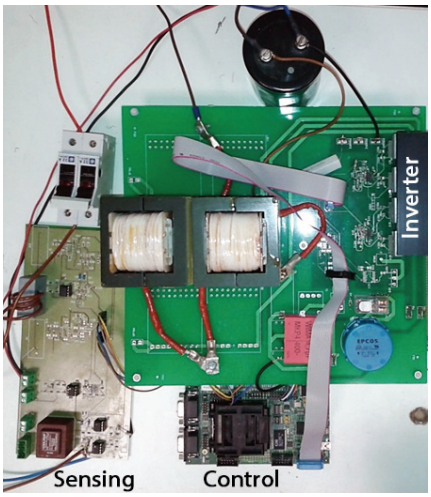

Figure 7. Experimental setup.

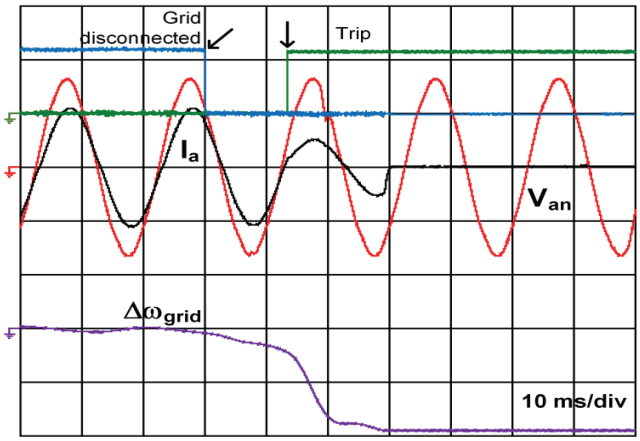

(a)

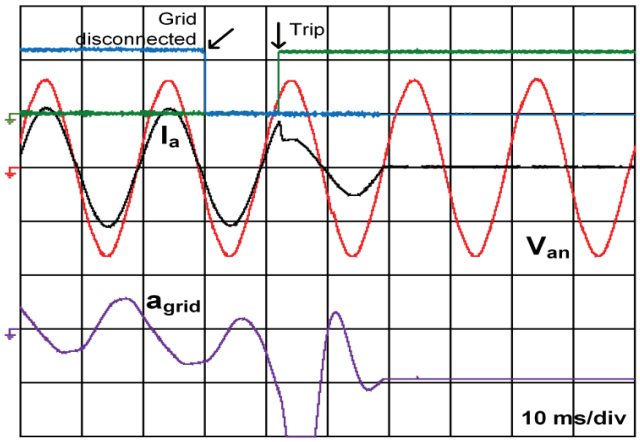

(b)

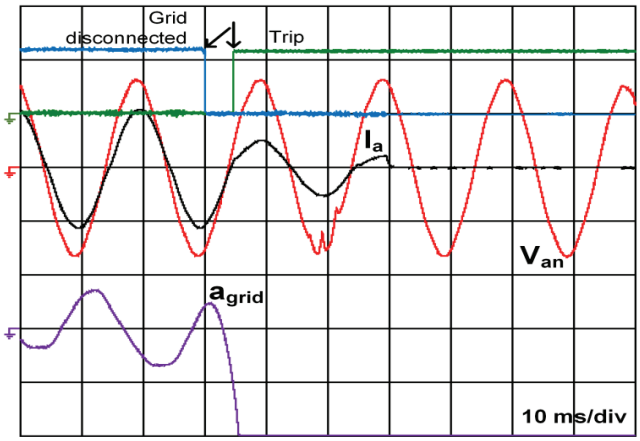

(c)

Figure 8. Experimental results with pure resistive load.

(a) SMS (b) ROCOF (c) SMS+ROCOF. Current 10 A/div, Voltage 200 V/div, grid frequency acceleration (a_{grid}) 10 rad/s^2/div, grid frequency variation ($\Delta\omega_{grid}$) 10 rad/s/div with zero at 2π50 rad/s.

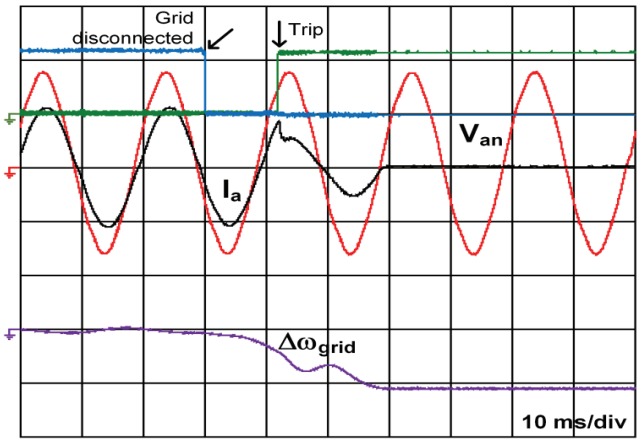

(a)

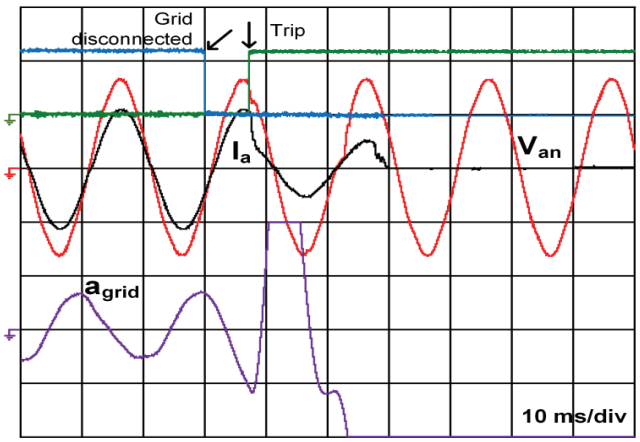

(b)

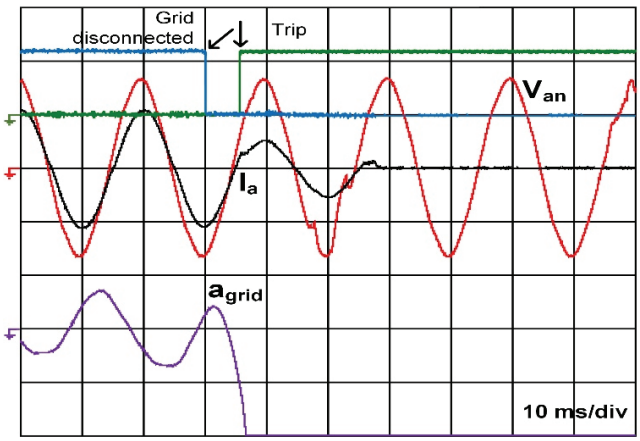

(c)

Figure 9. Experimental results with RLC resonant load.

(a) SMS (b) ROCOF (c) SMS+ROCOF. Current 10 A/div, Voltage 200 V/div, grid frequency acceleration (a_{grid}) 10 rad/s^2/div, grid frequency variation ($\Delta\omega_{grid}$) 10 rad/s/div with zero at 2π50 rad/s.

Table III summarizes the islanding detection times obtained with SMS, ROCOF and SMS+ROCOF. As it can be noticed, the use of the third-order SSLKF-PLL is able to produce detection times rather lower than those required by International Standards for different detection methods. In particular, the SMS+ROCOF active detection method produces the lowest detection times without having the inconvenience of NDZ. It is to notice that, using ROCOF passive method, the detection time intervals are lightly greater than SMS+ROCOF ones, whilst the power quality of the grid is not affected.

TABLE III. EXPERIMENTAL DETECTION TIMES INTERVALS

LOAD	SMS	ROCOF	SMS+ ROCOF
R=30Ω	13.9 ms	12.5 ms	5.5 ms
Q=1.4	12.4 ms	7.7 ms	6.2 ms

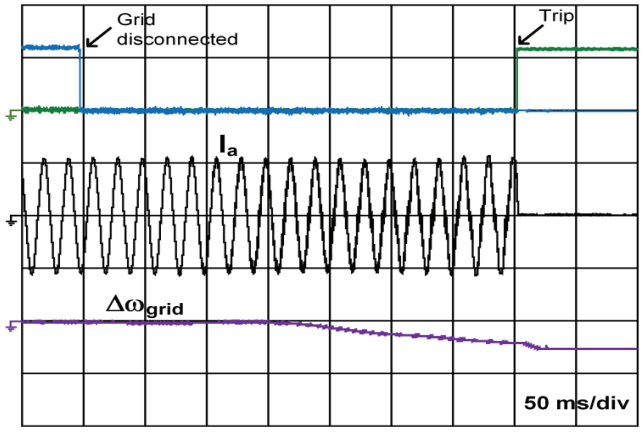

(a)

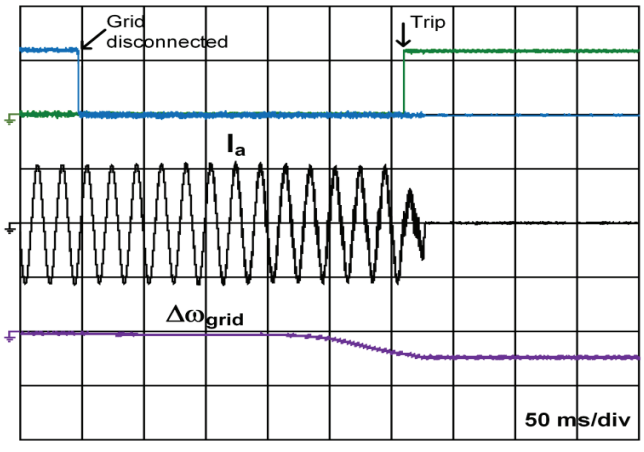

(b)

Figure 10. Experimental results for SRF-PLL with RLC resonant load. (a) AFD, (b) SMS. Current 10 A/div, grid frequency variation ($\Delta\omega_{grid}$) 10 rad/s/div with zero at $2\pi 50$ rad/s.

Finally, the proposed method has been experimentally compared versus two popular anti-islanding methods, based on the Single Reference Frame PLL (SRF-PLL) [26], namely Active Frequency Drift (AFD) and Slip Mode frequency Shift (SMS-SRF). To this aim, the same operating conditions as well as the same RLC load used to produce the results in Figure 9 have been accounted. The SRF-PLL bandwidth has been imposed equal to the SSLKF-PLL one (10Hz), while a 65Hz frequency drift has been set for AFD. Figure 10a and 10b show the achieved experimental results with the SRF-PLL using, respectively, AFD and SMS as an islanding detection method. As it is possible to observe, the detection time is equal to 356ms for AFD and equal to 264ms for SMS; thus, in both cases, the detection time is significantly greater than that obtained with the proposed method.

VI. CONCLUSIONS

The paper presents a performance comparison among different islanding detection methods, such as Rate Of Change Of Frequency (ROCOF), Slip Mode frequency Shift (SMS) and the combination of both SMS and ROCOF. All the methods have been evaluated using the estimations of the angle, frequency and angular acceleration provided by a Phase Locked Loop, based on a third-order Steady-State Linear Kalman Filter. Different tests have been performed, at first, on a simulation model, implemented in Matlab/Simulink, and then, experimentally, on a grid-connected inverter prototype. A Texas Instruments TMS320F28335 has been used to implement the inverter control and the islanding detectors. Such tests have been performed accounting RLC loads, with different Q values, as required by the most important international Standards. The proposed method has been also experimentally compared with the Active Frequency Drift and the Slip Mode frequency Shift, commonly used in combination with a standard Single Reference Frame PLL. The achieved results have confirmed the validity of the proposed approach, highlighting that the combination of SMS and ROCOF provides the fastest detection time interval among the considered methods.

REFERENCES

[1] IEEE Std. 929-2000, IEEE Recommended Practice for Utility Interface of Photovoltaic (PV) Systems, IEEE Standards Coordinating Committee on Photovoltaics, New York, NY, Apr. 2000

[2] IEEE Std. 1547, "IEEE Standard for Interconnecting distributed resources with electric power systems", 2003.

[3] IEEE Std. 1547.1, "IEEE Standard Conformance Test Procedures for Equipment Interconnecting Distributed Resources with Electric Power Systems", July 2005.

[4] IEC Std. 62116, "Test procedure of islanding prevention measures for utility-interconnected photovoltaic inverters", 2008.

[5] DIN-VDE Std. 0126-1-1, "Automatic Disconnection Device Between a Generator and the Low-Voltage Grid", 2006.

[6] CEI 0-21, "Reference technical rules for the connection of active and passive users to the LV electrical Utilities", June 2012.

[7] F. De Mango, M. Liserre, A. Dell'Aquila, A. Pigazo "Overview of Anti-Islanding Algorithms for PV Systems. Part I: Passive Methods" *Proc. of EPE-PEMC 2006*, Portoroz, Slovenia.

[8] F. De Mango, M. Liserre, A. Dell'Aquila, "Overview of Anti-Islanding Algorithms for PV Systems. Part II: Active Methods," *Proc. of EPE-PEMC 2006*, Portoroz, Slovenia.

[9] P. Mahat, C. Zhe, and B. Bak-Jensen, "Review of islanding detection methods for distributed generation," *Third International Conference on Electric Utility Deregulation and Restructuring and Power Technologies, DRPT 2008*, pp.2743,2748, April 2008.

[10] W. Bower and M. Ropp, "Evaluation of Islanding Detection Methods for Utility-Interactive Inverters in Photovoltaic Systems," Sandia National Labs., SANDIA REPORT SAND2002-3591, November 2002. [Online]. Available: http://prod.sandia.gov/techlib/access-control.cgi/2002/023591.pdf

[11] W. Bower and M Ropp, "Evaluation of islanding detection methods for photovoltaic utility-interactive power systems", *IEA Task V Report IEA-PVPS T5-09*, March 2002.

[12] Z. Ye, A. Kolwalkar, Y. Zhang, P. Du and R. Walling, "Evaluation of anti-islanding schemes based on non-detection zone concept", *IEEE Trans. on Power Electronics*, Vol. 19, No. 5, September 2004, p. 1171-1176.

[13] S. Jang and K. Kim, "An islanding detection method for distributed generations using voltage unbalance and total harmonic distortion of current," *IEEE Trans. on Power Delivery*, vol. 19, no. 2, pp. 745-752, April 2004.

[14] W. Freitas, Xu Wilsun, C.M. Affonso, H. Zhenyu, "Comparative analysis between ROCOF and vector surge relays for distributed generation applications," *IEEE Trans. on Power Delivery*, vol.20, no.2, pp.1315-1324, April 2005.

[15] A. Samui, and S.R. Samantaray, "Assessment of ROCPAD Relay for Islanding Detection in Distributed Generation," *IEEE Trans. on Smart Grid*, vol.2, no.2, pp.391-398, June 2011.

[16] A. V. Timbus, R. Teodorescu, F. Blaabjerg, U. Borup, "Online grid measurement and ENS detection for PV inverter running on highly inductive grid," *IEEE Power Electronics Letters*, vol. 2, no. 3, pp. 77-82, September 2004.

[17] M. Ciobotaru, V.G. Agelidis, R. Teodorescu, F. Blaabjerg, "Accurate and Less-Disturbing Active Antiislanding Method Based on PLL for Grid-Connected Converters," *IEEE Trans. on Power Electronics*, vol.25, no.6, pp.1576-1584, June 2010.

[18] Ropp, M.E., Begovic, M., Rohatgi, A., "Determining the Relative Effectiveness of Islanding Prevention Techniques Using Phase Criteria and Non-detection Zones," *IEEE Trans. on Energy Conversion,* vol. 15 no. 3, Sept. 2000, p. 290-296.

[19] S. Bifaretti, "Anti-islanding detector based on a robust PLL," *2013 IEEE Energy Conversion Congress and Exposition (ECCE)*, pp.2934-2940, 15-19 Sept. 2013.

[20] A. Bellini and S. Bifaretti, "Performances of a PLL Based Digital Filter for double-conversion UPS," *Proc of 13th Int. Conf. on Power Electronics and Motion Control Conference*, EPE-PEMC 2008, Poznan (Poland), September 2008.

[21] A. Bellini, S. Bifaretti, and V. Iacovone, "Robust PLL Algorithm for Three-Phase Grid-Connected Converters," *EPE Journal*, vol. 20, no. 4, December 2010.

[22] M. Ciobotaru, R. Teodorescu and F. Blaabjerg, "A new single-phase PLL structure based on second order generalized integrator", *Proc. of IEEE PESC*, pp. 1511-1516, 2006.

[23] D. Dong, Jin Li, D. Boroyevich, P. Mattavelli, I. Cvetkovic, and Y. Xue, "Frequency behavior and its stability of grid-interface converter in distributed generation systems," *Twenty-Seventh Annual Applied Power Electronics Conference and Exposition* (APEC), pp.1887-1893, 5-9 Feb. 2012.

[24] D. Dong, D. Boroyevich, P. Mattavelli, Bo Wen, and Y. Xue, "Anti-islanding protection in three-phase converters using grid synchronization small-signal stability," *2012 IEEE Energy Conversion Congress and Exposition* (ECCE), pp. 2712-2718, 15-20 Sept. 2012.

[25] S. Bifaretti, P. Zanchetta, A. J. Watson, L. Tarisciotti, and J.C. Clare, "Advanced Power Electronic Conversion and Control System for Universal and Flexible Power Management," *IEEE Trans. on Smart Grid*, vol. 2, no.2, pp. 231–243, June 2011.

[26] S. Chung, "A phase tracking system for three phase utility interface inverters," *IEEE Trans. on Power Electron*., vol. 15, no. 3, pp. 431–438, May 2000.